Structural phase transitions in Si and SiO_{2} crystals via the random phase approximation

Bing Xiao, Jianwei Sun, Adrienn Ruzsinszky, Jing Feng, and John P. Perdew

Phys. Rev. B **86**, 094109 — Published 14 September 2012

DOI: 10.1103/PhysRevB.86.094109

Structural Phase Transitions in Si and SiO_2 Crystals via the Random Phase Approximation

Bing Xiao,[1] Jianwei Sun,[1] Adrienn Ruzsinszky,[1] Jing Feng,[2] and John P. Perdew[1*]

[1]Department of Physics and Engineering Physics, School of Science and Engineering, Tulane University, New Orleans, Louisiana, 70118, USA

[2]Faculty of Materials Science and Engineering, Kunming University of Science and Technology, Kunming, 650093, P R China

We have assessed the performance of the non-selfconsistent random phase approximation (RPA) on two pressure-induced structural phase transitions, diamond to β-tin in Si and α-quartz to stishovite in SiO_2. The calculated equilibrium lattice properties of the four structures are in better agreement with experimental results than are those from several semilocal functionals. The energy differences between the high- and low-pressure phases are found to be 0.37 eV/Si and 0.39 eV/SiO_2, respectively. The transition pressure obtained from our RPA calculations for diamond to β-tin in Si is 12.2 GPa, in excellent agreement with the experimental value 11.3-12.6 GPa. However, the α-quartz to stishovite phase transition pressure in SiO_2 is found to be 5.6 GPa, lower than the experimental 7.46 GPa; the Perdew-Burke-Ernzerhof (PBE) semilocal functional gives the transition pressure closest to experiment in this case. We conclude that the non-selfconsistent nonlocal RPA accurately describes the insulator-to-metal transition in Si, where semilocal density functionals tend to fail. But the RPA error cancellation that is nearly perfect in many solids including Si may be less perfect in solid SiO_2, as it is in many molecules.

PACS number (s): 71.15.Mb 64.70.K- 81.30.-t

I. INTRODUCTION

The random phase approximation (RPA) is the simplest implementation of the adiabatic-connection fluctuation-dissipation theorem (ACFDT) density functional methods [1, 2]. As a result, it is often called RPA-ACFDT or RPA for simplicity. In a typical RPA calculation, the total energy has two different contributions, i.e., the Hartree-Fock energy and the RPA correlation energy:

$$E_t^{\mathrm{RPA}} = \underbrace{T_{KS}[n] + E_{\text{ion-el}} + E_H[n] + E_x\left[\{\psi_i^{KS}\}\right]}_{E_{HF}} \underbrace{- \int_0^1 d\lambda \int_0^\infty \frac{d\omega}{2\pi} \sum_{\vec{q}\in BZ} \sum_{\vec{G},\vec{G}'} v_{\vec{G},\vec{G}'}(\vec{q}) \left[\chi^{\lambda}_{\vec{G},\vec{G}'}(\vec{q},i\omega) - \chi^{0}_{\vec{G},\vec{G}'}(\vec{q},i\omega)\right]}_{E_c} , \quad (1)$$

where λ is the coupling constant that switches the Kohn-Sham non-interacting system ($\lambda = 0$) to the fully Coulomb-interacting system ($\lambda = 1$) at fixed electron density and $v_{\vec{G},\vec{G}'}(\vec{q}) = 4\pi e^2 / \left|\vec{q}+\vec{G}\right|^2 \delta_{\vec{G},\vec{G}'}$ is the bare Coulomb interaction between electrons represented in reciprocal space. In addition, $\vec{q}$ is a wavevector in the first Brillouin zone. $\vec{G}$ and $\vec{G}'$ are reciprocal lattice vectors. The Hartree-Fock energy E_{HF} consists of four terms: the non-interacting kinetic energy of the Kohn-Sham system ($T_{KS}[n]$), the electrostatic potential energy between electrons and ions ($E_{\text{ion-el}}$), the classic Coulomb or Hartree potential energy among electrons ($E_H[n]$), and the exact Hartree-Fock exchange energy ($E_x\left[\{\psi_i^{KS}\}\right]$) evaluated using Kohn-Sham occupied orbitals. In the correlation energy E_c, $\chi^{0}_{\vec{G},\vec{G}'}(\vec{q},i\omega)$ and $\chi^{\lambda}_{\vec{G},\vec{G}'}(\vec{q},i\omega)$ are the electron-density linear response functions of the non-interacting Kohn-Sham system and the λ-interacting system, respectively. The two response functions are connected with each other through a Dyson-like equation in reciprocal space [3].

$$\chi^{\lambda}_{\vec{G},\vec{G}'}(\vec{q},i\omega) = \chi^{0}_{\vec{G},\vec{G}'}(\vec{q},i\omega) + \sum_{\vec{G}_1,\vec{G}_2} \chi^{0}_{\vec{G},\vec{G}_1}(\vec{q},i\omega) \left[\frac{4\pi e^2 \lambda}{\left|\vec{q}+\vec{G}_1\right|^2}\delta_{\vec{G}_1,\vec{G}_2} + f^{\lambda}_{xc,\vec{G}_1,\vec{G}_2}(\vec{q},i\omega)\right] \chi^{\lambda}_{\vec{G}_2,\vec{G}'}(\vec{q},i\omega) , \quad (2)$$

In Eq. (2), $f^{\lambda}_{xc,\vec{G}_1,\vec{G}_2}(\vec{q},i\omega)$ is the short-range dynamical exchange-correlation kernel [2] which is ignored in RPA. For the correlation energy, the λ integration in Eq. (1) can be calculated analytically, and the remaining ω integration should be evaluated numerically for reciprocal lattice vectors up to the maximum kinetic energy

cutoff. Recently, the RPA-ACFDT method has been implemented in several *ab initio* codes non-selfconsistently. More details about the RPA-ACFDT theorem and its implementations can be found in references [3-5]. Thus the RPA method can be applied to realistic systems such as atoms, molecules, and crystal structures.

While RPA makes a substantial error of about -0.02 hartree/electron in the correlation energy, this error can cancel out of iso-electronic energy changes [6], and apparently does so for many properties of solids and surfaces. The finding of nearly-perfect error cancellation within RPA at the local density and gradient-corrected levels suggested [6] the use of RPA for realistic calculations.

Some earlier works on RPA calculations for *3d* transition metals [7], bulk materials [4, 8-12], defects [13], and surfaces [14] have already indicated the reliability and accuracy of the method. More recently, the pioneer works conducted by the Kresse group showed that RPA gives good geometrical properties and also heats of formation [4, 15]. For instance, the equilibrium lattice constants, bulk moduli, and cohesive energies of the tested metals, semiconductors, and insulators predicted by RPA are in better agreement with experimental results than those of semilocal functionals [4]. The RPA method was also successfully applied to van der Waals crystals in which long-range correlation plays a crucial role [9-12]; the failures of the local density approximation (LDA) and generalized gradient approximation (GGA) in these systems are well-known. In addition, Nguyen et al. [5] also discussed the results of bulk Si, the Be dimer, and atomic systems from RPA calculations, and their results confirmed the good quality of the RPA method for the ground state properties of these realistic systems. So far, the *selfconsistent* RPA method has only been tested for small atomic clusters [16]. For solids and molecules, these calculations usually start from either Kohn-Sham LDA (KS-LDA) orbitals or KS-GGA orbitals. In solids, the LDA and GGA potentials are usually close [4] to the RPA Kohn-Sham potential, "suggesting that self-consistency is a minor issue for extended systems".

The pressure-induced phase transition is an important topic in solid state physics and materials science. In our work, we investigated two pressure-induced phase transitions, namely the diamond (D-Si) to β-tin transition of Si and the α-quartz to stishovite transition of SiO_2. Exchange-correlation functionals at the LDA and GGA levels were applied to calculate the phase transition pressures of these two systems long ago [17-19], even at the all-electron level [19]. More recently, Hennig et al. [20] performed a thorough study on the D-Si to β-tin Si phase transition using exchange-correlation functionals from most rungs of Jacob's ladder except the RPA level. In that paper, the highest-level method was not RPA but the diffusion quantum Monte Carlo (DMC). From the calculated results, the

authors concluded that only the hybrid functional HSE06 and DMC can predict the transition pressure in excellent agreement with experiments for the D-Si to β-tin Si transition, and all tested semilocal functionals underestimate the phase transition energy difference and thus the transition pressure. In addition, Maezono et al. [21] calculated the D-Si to β-tin Si transition pressure by DMC using different pseudopotentials. Their results showed that the calculated transition pressure correlates with the choice of pseudopotential. Non-selfconsistent DMC calculations were also carried out for the SiO_2 phase transition in a recent paper [22]. Since the RPA method has been found to be a promising method for the ground-state properties of solids, we expect that RPA can predict the transition pressure between two polymorphs of a solid accurately.

The paper is organized as follows: Computational details about non-selfconsistent RPA method are given in section 2. Section 3 gives the RPA results for the phase transition properties of Si and SiO_2 systems, and discusses about the performance of the non-selfconsistent RPA method on phase transition. We give our conclusions in section 4.

II. COMPUTATIONAL DETAILS

Our calculations were performed using the Vienna ab-initio simulation program (VASP), where the RPA method is implemented non-selfconsistently [4, 23]. The projector augmented wave (PAW) method within the frozen-core approximation was employed for the pseudopotentials of Si and O atoms, i.e., Si_{3s3p3d} and O_{2s2p}, respectively [23]. The non-overlapping core radii for pseudo-Si and O atoms are 0.840 Å and 0.672 Å. The cutoff radii for generating partial waves for different angular quantum numbers, the number of partial waves and projectors of Si and O PAW potentials can be found in Ref. [3]. These special PAW pseudopotentials were built to describe the scattering properties of atoms accurately up to 10 Ry above the vacuum level. Their reliability and transferability have been extensively tested in Refs. [3] and [4]. We used GGA-PBE structures and orbitals as the initial input information for the following RPA calculations. In contrast to the conventional DFT calculations, the RPA total energy must be calculated separately as RPA correlation energy and Hartree-Fock energy, and both parts converge independently [4]. We have performed extensive tests on three parameters for the RPA method: kinetic energy cutoff (E_{cut}), k-mesh and E_{cut}^{GW}. The last parameter determines the size of the auxiliary plane wave basis for the response function, and the value is usually chosen to be between $E_{cut}/3$ and $2E_{cut}/3$ [3, 9]. From the convergence tests, we determined some parameters for the RPA calculations, given in Ref [24]. We found that for insulators or semiconductors such as SiO_2

and D-Si, both Hartree-Fock and RPA correlation energies converge rapidly under increase of the k-point mesh. The main error in the correlation energies is caused by the finite value of E_{cut}, because for semiconductors or insulators the RPA correlation energy usually converges as

$$E_c(E_{cut}) = E_c^{\infty} + \frac{A}{(E_{cut})^{3/2}} , \quad (3)$$

where E_c^{∞} is the converged RPA correlation energy and A is a fitting parameter which characterizes the error due to the finite E_{cut}. In our calculations, we found that the worst case was stishovite, where the absolute error without the extrapolation was predicted to be 20 meV/SiO_2. For the metallic β-tin Si phase, E_{HF} and E_c were always calculated using the same E_{cut} and k mesh. In addition, the long wave-length part ($\vec{q} \to 0$) of the exchange-correlation energy was excluded in RPA calculation for this phase in order to achieve the fastest convergence [4, 9]. For a system with a band gap, the calculations of E_{HF} and E_c energies with and without including the long wave-length part give almost the same results for the present calculation parameters. For instance, the difference for the calculated E_{total} (E_{total}=E_{HF}+E_c) by the two methods for D-Si phase is 2 meV/atom.

The phase transition parameters were also evaluated using several other semilocal and non-local functionals, including LDA [25], PBE [26], Perdew-Burke-Ernzerhof functional for solids (PBEsol) [27], Tao-Perdew-Staroverov-Scuseria meta-GGA functional (TPSS) [28], revised TPSS (revTPSS) [29], and Heyd-Scuseria-Ernzerhof hybrid functional (HSE06) [30].

III. RESULTS AND DISCUSSION

A. D-Si-to-β-Sn Si phase transition in silicon

In Figure.1, we show the calculated energy-volume curves for two polymorphs of SiO_2 and Si, respectively. The calculated energy-volume curves are relatively smooth, indicating that the present results are nearly-converged with respect to the k-point sampling in the irreducible wedge of the first Brillouin zone. The Birch-Murnaghan third-order equation of state (EOS) was used to fit the energy-volume data [31]. The equilibrium volume and bulk modulus for each phase were obtained from the same EOS parametric fitting, and the results are given in Table.1. One should note that the present RPA calculations are non-selfconsistent; therefore, the c/a ratios for alpha-quartz, stishovite and β-tin Si were fixed to the corresponding PBE values. Similar non-self consistent DMC calculations were also

applied to Si and SiO_2 systems in previous works [20, 22]. The transition pressure can be obtained by constructing the common tangent line for the two EOS-fitted energy-volume curves, and the results are also illustrated in Figure.1. The theoretical zero-point energy (ZPE) and finite-temperature (FT) phonon corrections to the Kohn-Sham phase transition pressure were also made in our paper, but only for the transition pressures in Table.2 below. Such corrections are usually evaluated from the phonon density of states [21, 32].

From Table.1, we can see that RPA predicts good equilibrium lattice properties of Si polymorphs. The lattice constant and bulk modulus of D-Si have been calculated by RPA in Ref [4], and the values are given as 5.432 Å and 99 GPa, respectively. Our RPA calculation gives 5.431 Å and 97.0 GPa for these two properties. The agreement between experimental results and RPA calculations is satisfactory for D-Si. Since the D-Si to β-tin Si transformation is kinematically reversible, the calculated equilibrium lattice properties of β-tin Si phase at 0 GPa can not be compared directly with experiments. However, the transition volume can be measured by experiment at the transition pressure. Using the Birch-Murnaghan third-order EOS, we also calculated this quantity and the results are given in Table.1. The obtained results are slightly larger than the measured ones for Si polymorphs. Hennig et al. [20] reported the transition volumes of Si polymorphs from diffusion Monte Carlo simulation (DMC); the values are also shown in Table.1. The RPA calculations are generally in agreement with DMC results. In addition, in the case of β-tin Si, our RPA value is slightly better than the DMC value when compared to experimental results.

The calculated phase transition parameters of Si system are given in Table.2. For the ZPE and FT correction to transition pressure, we simply cite the values from published results [21, 33]. The ZPE and FT correction (300 K) shift the D-Si to β-tin Si transition pressure by -1.3 GPa in Ref [33] and -1.0 GPa in a recent study [21]. For the D-Si to β-tin Si phase transition, RPA gives a good energy difference and transition pressure. Meanwhile, semilocal functionals underestimate the transition pressure, because the calculated energy difference is not sufficiently large to give the correct transition pressure. PBE and TPSS give better energy differences than other semilocal functionals. Moreover, both PBEsol and revTPSS predict the phase transition parameters less accurately than LDA. We also found that the calculated energy difference in RPA is situated between those of HSE06 and DMC. The obtained RPA transition pressure is in excellent agreement with experiments.

A reason why most semilocal functionals might perform badly for the D-Si to β-tin Si phase transition has been discussed in Ref [20]. Since D-Si is a semiconductor and β-tin Si is a metal, the phase transition from the former structure to the latter is an insulator-to-metal transformation. The electronic structures of the two Si polymorphs are

significantly different from each other. The well-known disadvantage of semilocal exchange-correlation functionals is that they usually underestimate physically-correct energy gaps for semiconductors and insulators because they miss the derivative discontinuity in the Kohn-Sham potential at integer electron number [34, 35]. Errors in the gap as a second difference of total energies are reflected by errors in the band gap in a *generalized* Kohn-Sham band structure [35]. (While the Kohn-Sham exchange-correlation potential is a functional derivative with respect to the density, the generalized one is with respect to the nondiagonal Kohn-Sham density matrix.) The abrupt change of band structure from the semiconducting D-Si phase to metallic β-Sn Si is associated with overlapping of the valence and conduction bands and shrinking of the band gap. Therefore, the nonlocal functionals such as HSE06 have an advantage in this case, because the band gap can be better described by them than by semilocal functionals [20, 36], and a larger gap presumably tends to stabilize the semiconducting D-Si phase with respect to the metallic β-tin phase. In this work, ACFDT-RPA calculation uses the exact exchange energy (EXX), and the non-local correlation part (RPA) is calculated using linear response theory from the GW approximation (GWA) [37]. The generalized Kohn-Sham band structure of the present method (EXX+RPA) would resemble the physically-meaningful GW_0 band structure [38]. As a result, the ground-state energy of the D-Si phase is equally well described by either HSE06 or RPA. Moreover, the ground-state properties of the β-tin Si phase are somewhat similar for different semilocal and nonlocal functionals. Thus the good performance of RPA on the D-Si to β-tin Si phase transition can be explained.

B. α-quartz-to-stishovite phase transition in silica

For the SiO_2 system, the RPA also gives a good equilibrium cell volume for the α-quartz phase, where it only slightly underestimates the equilibrium cell volume by 0.13 %. However, the calculated bulk modulus of α-quartz is obviously larger than the experimental value. Hamann et al. [18] used both LDA and PBE to calculate the bulk modulus of α-quartz and stishovite. Interestingly, the RPA calculation overestimates the bulk modulus of α-quartz by the same amount as in LDA and PBE. In contrast to α-quartz, RPA gives a good bulk modulus for stishovite, but the equilibrium cell volume is overestimated. One should bear in mind that the present RPA calculations are non-selfconsistent, and the input structures were optimized using PBE. From Table.1, we can see that for α-quartz the c/a ratio obtained from PBE agrees less well with experiment than for stishovite. The c/a ratio of stishovite deviates from the corresponding experimental value by -0.2 %, and that of α-quartz is -0.4 %. Recently, the DMC method has been applied to calculate the phase transition properties of SiO_2 polymorphs at ultrahigh pressures [22], and the

DMC also gave similar results to our RPA calculations for α-quartz and stishovite. It can be seen clearly from Table.1 that DMC and RPA actually predict the same equilibrium cell volume for stishovite.

In Table.2, we show the calculated phase transition parameters for SiO_2. It is found that the transition pressure from α-quartz to stishovite is increased by 0.57 GPa after including ZPE and FT correction (300 K). The positive shift of the transition pressure is reasonable, because the entropy of α-quartz is significantly larger than stishovite [39]. As a result, the increase of temperature somewhat stabilizes α-quartz over stishovite due to the entropy. For the α-quartz to stishovite phase transition, PBE gives the best phase transition parameters, and the results are comparable to the benchmark DMC calculations [22]. The transition pressures calculated by two meta-GGA functionals named TPSS and revTPSS are less accurate than PBE results. The hybrid functional HSE06 performs well for SiO_2 and the corresponding phase transition parameters are similar to DMC results. However, for the same system, RPA shows relatively poor performance for transition parameters compared to DMC, HSE06, and PBE. The calculated non-selfconsistent RPA energy difference between α-quartz and stishovite is smaller than the experimental value by 26.8 %. (RPA selfconsistency might reduce this error, if it lowered the energy more for the lower-symmetry α-quartz structure.) Therefore, the estimated non-selfconsistent RPA α-quartz to stishovite transition pressure is too small. The results shown in Table.2 for SiO_2 also indicate that both RPA and TPSS give similar values for the energy differences between stishovite and α-quartz. However, the transition pressure predicted by RPA is larger than that of TPSS; the main reason is that TPSS gives a too-large equilibrium cell volume for the quartz phase. Similarly, PBE gives the best energy difference for SiO_2, but the cell volumes of both phases are overestimated, especially for α-quartz.

The good performance of nonlocal RPA for the equilibrium cell volume of α-quartz is partly related to the van der Waals interaction in the structure. The RPA captures the van der Waals interaction in various solids, including the strongly polarizable covalent and ionic solids and molecular crystal structures. For stishovite, the main reason for the observed discrepancies between the experimental cell volume and those of DMC and RPA is not clear at the moment. Does the underestimation of the energy difference by RPA arise from fixing the c/a ratios of α-quartz and stishovite at their PBE values? The previous tests of the non-selfconsistent RPA algorithm on simple cubic solids give equilibrium lattice constants in good agreement with experiments [4]. Whether this is also true for low-symmetry crystal structures (like α-quartz with four internal degrees of freedom associated with atomic positions) is not known. In Figure.2, we show the calculated energy landscapes of SiO_2 structures near their equilibrium

geometries. The results indicate that the present RPA method does not provide satisfactory equilibrium properties (cell volume and c/a ratio) for SiO_2 system. From the energy landscapes shown in Figure.2, the estimated energy difference between stishovite and α-quartz is even smaller than that given by using PBE geometries. Notice that in calculating the energy landscapes for SiO_2 phases, the internal degrees of freedom were relaxed using the PBE functional.

A likelier possibility is that low symmetry solids are more like molecules, in which the errors of the RPA correlation energy cancel out of iso-electronic energy differences less perfectly than they do for high symmetry solids [40, 41]. Ruzsinszky et al. [42] pointed out that the isoelectronic energy differences in solids are typically well-described by either RPA or RPA+, but a global hybrid functional such as $E_{total}(\text{Hybrid})=\frac{1}{2}E_{total}(\text{PBE})+\frac{1}{2}E_{total}(\text{RPA})$ is more accurate for calculating the isoelectronic energy changes in molecules. In order to verify our conjecture on the molecular nature of SiO_2 phases due to their low symmetry, we have recalculated the energy differences for Si and SiO_2 systems roughly using $\Delta E(\text{Hybrid})=\frac{1}{2}\Delta E(\text{PBE})+\frac{1}{2}\Delta E(\text{RPA})$, and the corresponding values are 0.33 eV/atom and 0.46 eV/SiO_2, respectively. We can see that the calculated energy difference is improved for SiO_2, but it is worsened for Si.

IV. CONCLUSIONS

In summary, we have studied the phase transition parameters of the α-quartz to stishovite and D-Si to β-tin Si phase transformations using non-selfconsistent RPA calculations in the VASP code. The obtained equilibrium lattice volumes of most structures are in good agreement with DMC (or QMC) simulations and experimental results. The calculated phase transition pressure and transition volume of Si are also in excellent agreement with experimental values. On the other hand, the energy difference between α-quartz quartz and stishovite is underestimated by RPA and thus the corresponding transition pressure is smaller than those of experiment and several other local and nonlocal functionals. While non-selfconsistent RPA seems to work well for the difficult insulator-to-metal transition in Si, selfconsistent and geometry-optimized RPA calculations may be needed for the low-symmetry crystal structures of SiO_2. While non-selfconsistent RPA seems to work well for the difficult insulator-to-metal transition in Si, the RPA error cancellation may be less perfect in SiO_2, as in molecules.

ACKNOWLEDGMENTS

This work was supported by the National Science Foundation under Grant No, DMR-0854769, and by the Department of Energy under Grant No. DE-SC0007989. Most of our calculations were carried out using the workstation clusters provided by the Louisiana Optical Network Initiative (LONI: http://www.loni.org/) and also by the Center for Computational Science at Tulane University.

References

[1] D.C. Langreth and J.P. Perdew, Phys. Rev. B **21**, 5469 (1980).

[2] M. Lein, E.K.U. Gross, and J.P. Perdew, Phys. Rev. B **61**, 13431 (2000).

[3] J. Harl, PhD thesis. Universität Wien, Austria (2008).

[4] J. Harl, L. Schimka, and G. Kresse, Phys. Rev. B **81**, 115126 (2010).

[5] H.-V. Nguyen and S. de. Gironcoli, Phys. Rev. B **79**, 205114 (2009).

[6] Z. Yan, J.P. Perdew, and S. Kurth, Phys. Rev. B **61**, 16430 (2000).

[7] T. Kotani and H. Akai, J. Mag. Mag. Mater. **177-181**, 569 (1998).

[8] P.G. Gonzalez, J.J. Fernandez, A. Marini, and A. Rubio, J. Phys, Chem. A **111**, 12458 (2007).

[9] J. Harl and G. Kresse, Phys. Rev. B **77,** 045136 (2008).

[10] D. Lu, Y. Li, D. Rocca and G. Galli, Phys. Rev. Lett. **102**, 206411 (2009).

[11] Y. Li, D. Lu, H.-V. Nguyen and G. Galli, J. Phys. Chem. A **114.** 1944 (2010).

[12] H.-V. Nguyen and G. Galli, J. Chem. Phys. **132**, 044109 (2010) .

[13] F. Bruneval, Phys. Rev. Lett. **108**, 256403 (2012).

[14] L. Schimka, J. Harl, A. Stroppa, A. Gruneis, M. Marsman, F. Mittendorfer, and G. Kresse, Nature Materials **9**, 741 (2010).

[15] J. Harl and G. Kresse, Phys. Rev. Lett. **103**, 056401 (2009).

[16] M. Hellgren, D.R. Rohr, and E.K.U. Gross, J. Chem. Phys. **136**, 034106 (2012)

[17] K.J. Chang and M.L. Cohen, Phys. Rev. B **31**, 7819 (1985).

[18] D.R. Hamann, Phys. Rev. Lett. **76**, 660 (1996).

[19] A. Zupan, P. Blaha, K. Schwarz, and J.P. Perdew, Phys. Rev. B **58**, 11266 (1998).

[20] R.G. Hennig, A. Wadehra, K.P. Driver, W.D. Parker, C.J. Umrigar, and J.W. Wilkins, Phys. Rev. B **82**, 014101 (2010).

[21] R. Maezono, N.D. Drummond, A. Ma, and R.J. Needs, Phys. Rev. B **82**, 184108 (2010).

[22] K.P. Driver, R.E. Cohen, Z. Wu, B. Militzer, P. Lopez. Rios, M.D. Towler, R.J. Needs, and J.W. Wilkins, Proc. Nat. Acad. Sci. (USA) **107**, 9519 (2010)

[23] G. Kresse and D. Joubert, Phys. Rev. B **59**, 1758 (1999).

[24] Supplementary materials.

[25] J.P. Perdew and A. Zunger, Phys. Rev. B **23**, 5048 (1981).

[26] J.P. Perdew, K. Burke, and M. Ernzerhof, Phys. Rev. Lett. **77**, 3865 (1996).

[27] J.P. Perdew, A. Ruzsinzky, G.I. Csonka, O.A. Vydrov, G.E. Scuseria, L.A. Constantin, X. Zhou, and K. Burke, Phys. Rev. Lett. **100**, 136406 (2008)

[28] J. Tao, J.P. Perdew, V.N. Staroverov, and G.E. Scuseria, Phys. Rev. Lett. **91**, 146401 (2003).

[29] J.P. Perdew, A. Ruzsinszky, G.I. Csonka, L.A. Constantin, and J. Sun, Phys. Rev. Lett. **103**, 026403 (2009).

[30] J. Heyd, G.E. Scuseria, and M. Ernzerhof, J. Chem. Phys. **118**, 8207 (2003).

[31] A. Otero-de-la Roza, D. Abbasi-Pérez, and V. Luaña, Comput. Phys. Comm**. 182**, 1708 (2011).

[32] The phonon spectra of quartz and stishovite were calculated using the CASTEP code. The crystal structures were fully optimized and norm-conserving-type pseudopotentials were used for the pseudo-atoms. The kinetic energy cutoff value for the plane wave expansions was set to 550 eV and the k-point mesh were 6×6×8 and 4×4×4 for stishovite and α-quartz, respectively. The PBE functional was employed in the calculations.

[33] K. Gaál-Nagy, A. Bauer, M. Schmitt, K. Karch, P. Pavone, and D. Strauch, Phys. Status Solidi B **211**, 275 (1999).

[34] J.P. Perdew, R.G. Parr, M. Levy, and J.L. Balduz, Jr., Phys. Rev. Lett. **49**, 1691 (1982).

[35] J.P. Perdew and M. Levy, Phys. Rev. Lett. **51**, 1884 (1983).

[36] A.J. Cohen, P. Mori-Sánchez, and W. Yang, Science. **321**, 792 (2008).

[37] M. Shishkin and G. Kresse, Phys. Rev. B **74**, 035101 (2006).

[38] M. Grüning, A. Marini, and A. Rubio, J. Chem. Phys. **124**, 154108 (2006).

[39] C. Lee and X. Gonze, Phys. Rev. B **51**, 8610 (1995).

[40] F. Furche, Phys. Rev. B. **64**, 195120 (2001).

[41] A. Ruzsinszky, J.P. Perdew, and G.I. Csonka, J. Chem. Phys. **134**, 114110 (2011).

[42] A. Ruzsinszky, J.P. Perdew and G.I. Csonka, J. Chem. Theory Comput., **6**, 127 (2010).

Table.1 Equilibrium lattice properties of Si and SiO_2 polymorphs from RPA calculations, including cell volume (V), c/a ratio, bulk modulus (B), pressure derivative of bulk modulus (B`) and transition volume (V_t). The results are compared with experimental values and also with DMC calculations

Structure	Properties	RPA	Exp[a]	DMC[a]	Structure	Properties	RPA	Exp[a]	DMC[a]
D-Si	V (Å^3/cell)	160.17	160.00	159.84	β-tin Si	V (Å^3/cell)	60.99	—	60.08
	c/a	1.0000	1.0000	1.0000		c/a	0.5487	0.5500	0.5500
	B (GPa)	97.0	99.2	98.0		B (GPa)	113.5	—	107.0
	B`	4.84	4.11	4.60		B`	4.27	—	4.60
	V_t (Å^3/Si)	18.19	18.15	18.14		V_t (Å^3/Si)	13.99	13.96	13.90
			Exp[b]	DMC[c]				Exp[b]	DMC[c]
α-quartz	V (Å^3/cell)	113.26	113.41	113.44	Stishovite	V (Å^3/cell)	47.32	46.65	47.34
	c/a	1.0950	1.0995	—		c/a	0.6373	0.6387	—
	B (GPa)	44.8	38.0	32.0		B (GPa)	311.7	313.0	305.0
	B`	4.89	6.0	7.0		B`	4.26	2.8~6.0	3.7
	V_t (Å^3/SiO_2)	31.81	—	—		V_t (Å^3/SiO_2)	22.85	—	—

[a]Reference [20]

[b]Reference [18]

[c]Reference [22]

Table.2 Evaluated energy differences and transition pressures of Si and SiO_2 systems. The energy difference is defined as $E=E_{HP}-E_{LP}$, where HP and LP refer to high and low pressure phases, respectively. The zero-point energy and finite temperature (300 K) corrections are only made for the calculated P_{tr} values, as explained in the text.

	Properties	LDA	PBEsol	PBE	TPSS	revTPSS	HSE06	RPA	DMC[a]	Exp
Si	E (eV/atom)	0.21	0.19	0.29	0.27	0.16	0.40	0.37	0.42	—
	P_{tr} (GPa)	6.0	5.1	8.7	7.6	4.0	13.6	12.2	14.0± 1.0 DMC[b]	11.3-12.6[a]
SiO_2	E (eV/ SiO_2)	-0.03	0.17	0.53	0.38	0.19	0.49	0.39	0.50	0.51-0.54[c]
	P_{tr} (GPa)	—	2.7	7.0	3.9	2.7	6.1	5.6	6.2~6.5	7.46[c]

[a]Reference [20]

[b]Reference [22]

[c]Reference [18]

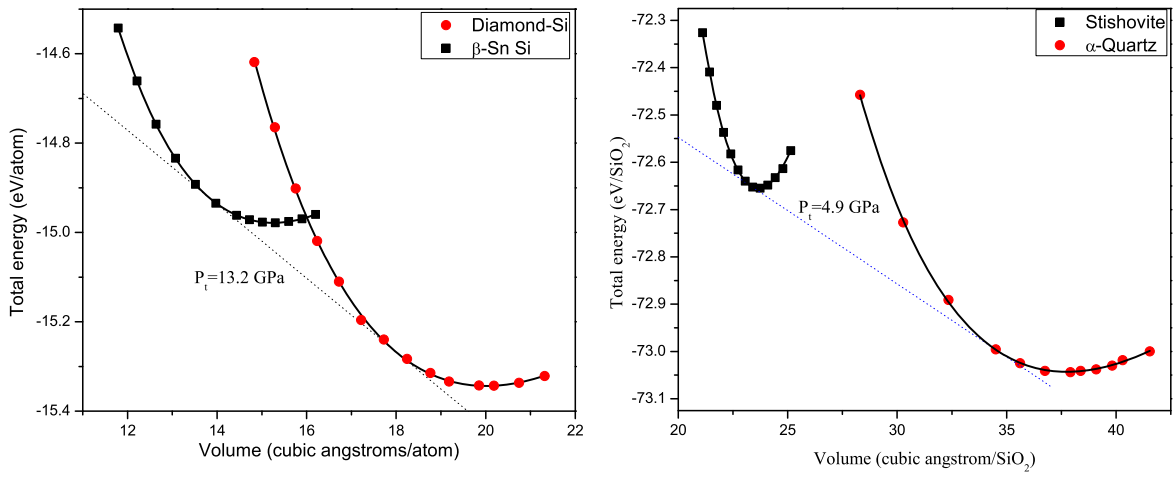

(a) (b)

Figure.1 (Color online) The energy versus volume curves of the Si and SiO_2 systems. The dotted line is the common tangent line obtained from the Birch-Murnaghan third-order EOS, and the solid lines in the graphs are fitted to the data points by the same EOS: (a): Si; (b): SiO_2.

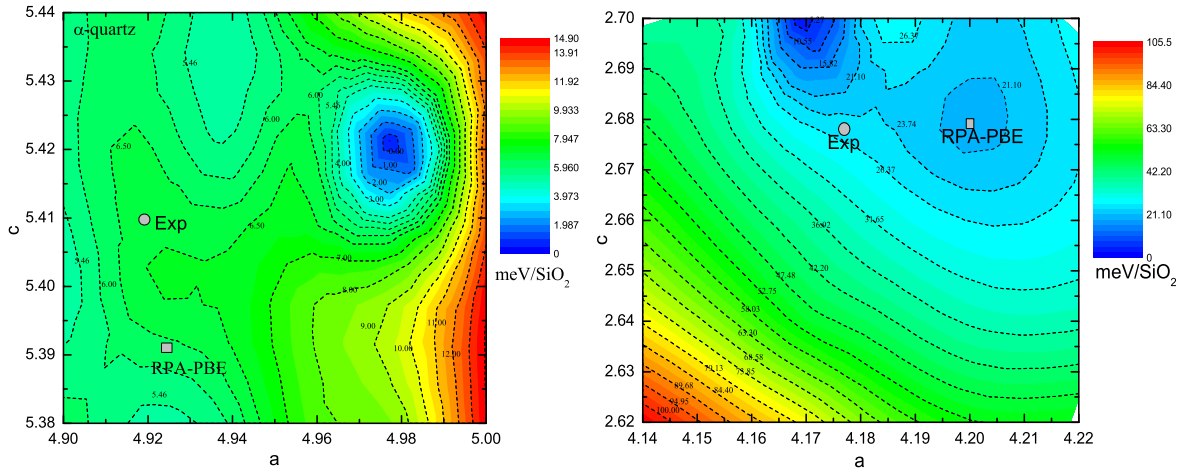

(a) (b)

Figure.2 (Color online) Calculated RPA energy landscapes of SiO_2 phases, with all geometry parameters other than the lattice constants c and a from PBE. The energy minimum is in the darkest blue area. The experimental lattice constants are indicated by gray circles. The gray squares show the lattice constants found by minimizing the RPA energy with respect to a only, at fixed PBE c/a. The unit for lattice constants is Å. The local minimum is chosen to be the zero reference energy: (a): α-quartz b): stishovite. (Unlike SiO_2, Si has no internal geometry parameter.)